PHILOSOPHICAL TRANSACTIONS A

Phil. Trans. R. Soc. A.
doi:10.1098/not yet assigned

Strong Magnetic Exchange and Frustrated Ferrimagnetic Order in a Weberite-Type Inorganic-Organic Hybrid Fluoride

L. Clark[1*], M. Albino[2,5], V. Pimenta[2,5], J. Lhoste[2], I. da Silva[3], C. Payen[4], J.-M. Grenèche[2], V. Maisonneuve[2], P. Lightfoot[5] and M. Leblanc[2]

[1]*Department of Chemistry and Materials Innovation Factory, University of Liverpool, 51 Oxford Street, Liverpool L7 3NY, UK*

[2]*Institut des Molécules et Matériaux du Mans (IMMM) UMR CNRS 6283, Le Mans Université, Avenue Olivier Messiaen, 72085 Le Mans Cedex 9, France*

[3]*ISIS Facility, Rutherford Appleton Laboratory, Chilton, Didcot, Oxford, OX11 0QX, UK*

[4]*Institut des Matériaux Jean Rouxel (IMN), UMR CNRS 6502, Université de Nantes, 2 rue de la Houssinière, BP 32229, 44322 Nantes Cedex 3, France*

[5]*School of Chemistry and EaStCHEM, University of St Andrews, St Andrews, Fife KY16 9ST, UK*

Keywords: coordination frameworks, fluorides, neutron diffraction, ^{57}Fe Mössbauer spectrometry.

Abstract

We combine powder neutron diffraction, magnetometry and ^{57}Fe Mössbauer spectrometry to determine the nuclear and magnetic structures of a strongly interacting weberite-type inorganic-organic hybrid fluoride, $Fe_2F_5(Htaz)$. In this structure, Fe^{2+} and Fe^{3+} cations form magnetically frustrated hexagonal tungsten bronze (HTB) layers of corner sharing octahedra. Our powder neutron diffraction data reveal that, unlike its purely inorganic fluoride weberite counterparts which adopt a centrosymmetric *Imma* structure, the room-temperature nuclear structure of $Fe_2F_5(Htaz)$ is best described by a non-centrosymmetric *Ima*2 model with refined lattice parameters a = 9.1467(2) Å, b = 9.4641(2) Å and c = 7.4829(2) Å. Magnetic susceptibility and magnetisation measurements reveal that strong antiferromagnetic exchange interactions prevail in $Fe_2F_5(Htaz)$ leading to a magnetic ordering transition at T_N = 93 K. Analysis of low-temperature powder neutron diffraction data indicates that below T_N, the Fe^{2+} sublattice is ferromagnetic, with a moment of 4.1(1) μ_B per Fe^{2+} at 2 K, but that an antiferromagnetic component of 0.6(3) μ_B cants the main ferromagnetic component of Fe^{3+}, which aligns antiferromagnetically to the Fe^{2+} sublattice. The zero-field and in-field Mössbauer spectra give clear evidence of an excess of high-spin Fe^{3+} species within the structure and a non-collinear magnetic structure.

Introduction

Inorganic fluorides are increasingly recognised for their unique physical properties,[1] including intriguing magnetic behaviours,[2] multiferroicity,[3] and ionic conductivity.[4] Even so, inorganic fluorides and fluoride minerals tend to remain relatively understudied in comparison to their oxide counterparts. In particular,

*Lucy Clark (lucy.clark@liverpool.ac.uk).

regarding their magnetic properties, a common preconception is that the extreme electronegativity of the fluoride anion leads to less pronounced magnetic interactions in metal fluorides than in analogous metal oxides. However, the superexchange coupling of ~ 1000 K in the Ag^{2+} fluoride, $KAgF_3$, certainly challenges this traditional notion, and far exceeds the typical energy scales of magnetic exchange in most inorganic oxides.[5]

Of course, another widely celebrated class of materials that has emerged in recent years are inorganic-organic hybrid coordination frameworks, such as metal-organic frameworks (MOFs). These extended solids of metal ion centres connected via organic linker molecules result in porous structures with cavities in which cations, solvated species or gas molecules can be inserted. Numerous useful properties result from these features, including catalysis,[6] gas storage or separation,[7] and drug delivery.[8] However, the magnetic properties of such coordination frameworks also tend to be less well-explored, again, arguably due to the generalisation that their less dense crystal structures disfavour the cooperative magnetic phenomena inherent to conventional inorganic solids. Excitingly, a growing number of research groups are working to dispel this idea, with a rich diversity of magnetic behaviours in coordination frameworks now beginning to capture the imagination of the magnetism community more widely.[9-12] For instance, there are a few cases of inorganic-organic hybrid framework materials that have sufficiently dense structures that the magnetic ordering of their paramagnetic metal ion centres occurs above liquid nitrogen temperatures. Several prime examples are to be found within an extensive series of weberite-type inorganic-organic hybrid fluorides, $M^{2+}M^{3+}F_5$(H*taz*), where M^{2+} = Mn, Fe, Co, Ni, Cu, Zn, M^{3+} = Ti, V, Mn, Fe, Ga and H*taz* is the organic linker 1,2,4-triazole.[13,14] These hybrid frameworks, isostructural with $ZnAlF_5$(H*taz*),[15] were recently reported by us to adopt an orthorhombic *Imma* structure at room temperature, closely related to that of the fluoride mineral weberite, $Na_2M^{2+}M^{3+}F_7$,[16-18] and $Fe_2F_5(H_2O)_2$.[19,20] The weberite structure is composed of intersecting and almost perpendicular hexagonal tungsten bronze (HTB) layers (Figure 1a), characterised by triangles of corner-sharing M^{2+} and M^{3+} octahedra (Figure 1b). More specifically, each of the cation triangles within the HTB layers is occupied by two M^{3+} cations and one M^{2+} cation such that each M^{3+} and M^{2+} cation belongs to four and two triangles, respectively. All fluoride weberites with paramagnetic M^{2+} and M^{3+} cations are known to exhibit dominant antiferromagnetic exchange interactions and, as such, an inherent geometric frustration of the magnetic interactions within the HTB layers of such systems is expected.[21]

In our previous publication, we demonstrated – by magnetometry measurements and ^{57}Fe Mössbauer spectrometry – that four compounds within this series of weberite-type inorganic-organic hybrid fluorides with three-dimensional magnetic connectivity order magnetically at temperatures significantly higher than is typical of magnetic coordination frameworks.[13] Those based on cation groups of $Fe^{2+}/Fe^{3+}/Ga^{3+}$, Co^{2+}/Fe^{3+}, Mn^{2+}/Fe^{3+} and $Mn^{2+}/Fe^{2+}/Fe^{3+}$ order magnetically at 80 K, 82 K, 100 K and 102 K, respectively, each with a net ferrimagnetic behaviour below T_N. In the hybrid frameworks based on cations with strong magnetocrystalline anisotropy – Co^{2+} and Fe^{2+} – the direction of the magnetisation was observed to switch depending on the thermal and magnetic history of the sample. Interestingly, this behaviour is not seen in the fluoride mineral weberites, $Na_2M^{2+}M^{3+}F_7$, based on the same cation couples,[22] and so appears unique to the hybrid framework analogues. As such, further investigation of the cooperative magnetic properties of this family of strongly interacting hybrid coordination frameworks, and a careful comparison of their features to those of their inorganic fluoride counterparts are worthwhile pursuits. Here, we exploit the sensitivity of neutrons to the light elements within the structure of these hybrid coordination frameworks, carbon, nitrogen and particularly hydrogen, as well as to the presence of an electronic moment of metal cations, to accurately determine the nuclear structure of the Fe_2F_5(H*taz*) member of this series and follow the evolution of magnetic order below T_N. In addition, we correlate the nuclear and magnetic structures of Fe_2F_5(H*taz*) determined by variable temperature powder neutron diffraction with the results of the magnetometry measurements and ^{57}Fe Mössbauer spectrometry.

Experimental Methods

Phase pure, polycrystalline $Fe_2F_5(Htaz)$ was synthesised by a microwave-assisted solvothermal method in ethanol from FeF_2, FeF_3, 4 % aqueous HF and 1,2,4-triazole (H*taz*) at 160°C. We note that it was not necessary to deuterate our polycrystalline sample and that even with a hydrogen-containing material, we were able to obtain powder neutron diffraction data of sufficiently good quality for our analysis. Magnetometry measurements were performed on a Quantum Design SQUID Magnetic Properties Measurement System (MPMS) in applied fields of 0.1, 1 and 5 T. Susceptibility data were recorded over the temperature range 2 – 300 K in zero field cooled (ZFC) and field cooled (FC) conditions. Magnetic hysteresis cycles were taken between –7 and +7 T. The molar diamagnetic contribution to the data was corrected by applying Pascal's constants, and the contribution of the sample holder has been removed from the data. ^{57}Fe Mössbauer spectroscopy experiments were performed in transmission geometry with a 925 MBq γ-source of ^{57}Co/Rh mounted on a conventional constant acceleration drive. The spectra were recorded between 10 – 300 K using either a bath cryostat or a cryomagnetic device generating an applied field parallel to the γ-beam. Data were analysed in the MOSFIT program, fitting quadrupolar and magnetic components of Lorentzian profile lines. α-Fe was used as a reference standard and the isomer shift values are quoted to that of α-Fe. Powder neutron diffraction data were collected on the GEM diffractometer at the ISIS Neutron and Muon Facility. 1 g of polycrystalline sample was packed into a 6 mm vanadium can and loaded into a He cryostat. Data were collected on warming in the range of 1.5 – 300 K, counting for approximately 2 hours per temperature. Data were analysed in multi-bank refinements using the GSAS software. For each diffraction pattern, the background was modelled by a shifted Chebyshev polynomial function. The DIFA diffractometer constant was refined (except for Bank 1, where it was kept fixed), along with profile parameters σ_1 and γ_1 of pseudo-Voigt time-of-flight peak shape function. The time-of-flight absorption correction model in GSAS was also applied during the data analysis.

Results and Discussion

Nuclear Structure of $Fe_2F_5(Htaz)$

The powder neutron diffraction data of $Fe_2F_5(Htaz)$ were collected on all six detector banks of the GEM diffractometer at 300 K (Figure 2). At this temperature, the diffraction data can be indexed in the centrosymmetric orthorhombic space group *Imma*, and Rietveld analysis of the *Imma* structural model determined previously from X-ray diffraction yields a good fit to the powder neutron diffraction data with a total weighted *R*-factor, R_{wp} = 1.37 %. However, within this model, the isotropic thermal displacement of the hydrogen atoms at the H1 site of H*taz* linker molecules are unusually large at 300 K (Table 1), and, unexpectedly, increase upon cooling from 150 K (H1 U_{iso} = 0.063(2) Å^2) to 100 K (H1 U_{iso} = 0.075(4) Å). In an attempt to account for this anomalous behaviour, we subsequently applied an anisotropic treatment of the thermal displacements of the H*taz* atoms within the *Imma* structure at 300 K. Not only was the refinement stable, but it also gave a significant improvement in the quality of the overall fit, with R_{wp} = 1.11 %. In this model, we maintain isotropic thermal displacements for the Fe and F sites, however, as we find a physically reasonable temperature variation for these parameters. Interestingly, what this anisotropic model refinement reveals is a large elongation of the thermal ellipsoids of the H*taz* atoms along the *b*-axis of the *Imma* unit cell and significant displacement of the linker atoms out of the (010) mirror plane. Consequently, the loss of this symmetry element leads to a distortion of the *Imma* structure to the non-standard and non-centrosymmetric *Im*2*a* space group. As such, by inversion of the *b*- and *c*-axes and a shift of the atomic positions of the non-standard setting, we can arrive at a model for the distorted structure in the standard space group setting, *Ima*2. By comparison, it is worth noting that the inversion symmetry of inorganic fluoride weberites, Na_2NiFeF_7 and Na_2NiAlF_7,[23,24] and $M^{2+}FeF_5(H_2O)_2$ (M^{2+} = Mn, Fe, Zn),[25,26] was also questioned in the early literature, with initial

proposals for the weberite structure in both centrosymmetric *Imma* and non-centrosymmetric *Imm*2 space groups. However, it was subsequently confirmed that, when observed, (*hk*0) reflections with $h(k) \neq 2n$ that led to the *Imm*2 space group assignment were only present due to a double diffraction Renninger effect.[23]

In the present case, on the other hand, not only does Rietveld fitting the isotropic *Ima*2 model to the 300 K data (Figure 2) allow for a modest improvement of the refinement reliability over the isotropic *Imma* model (total R_{wp} = 1.26 %) but, more importantly, all isotropic thermal displacement values are now acceptable (Table 2). This nuclear structure refinement result is also confirmed for $Fe_2F_5(Htaz)$ at 150 K (R_{wp} = 1.53 %) and 100 K (R_{wp} = 2.40 %) with isotropic thermal parameters of the hydrogen atom at the H1 site of U_{iso} = 0.024(2) Å^2 and U_{iso} = 0.015(3) Å^2, respectively. A projection of the *Ima*2 crystal structure appears in Figure 1, with a list of selected bond distances and angles taken from the model refinement to data at 300 K given in Table 3. The mean Fe1-F and Fe2-F distances are consistent with Fe^{3+}-F and Fe^{2+}-F distances in FeF_3 and FeF_2, respectively,[27,28] and the Fe-F-Fe angles – which ultimately govern the nature of magnetic interactions – are close to 145 °. Bond distance calculations indicate that the N2-H2···F1 hydrogen bonds are fairly strong with N···F distances of 2.843(3) Å and N-H···F angles of 155.8(9) °. Conversely, the C-H···F hydrogen bonds are weak, with a bond length of 3.204(7) Å and a C-H···F bond angle of 168.7(2) °.

Magnetometry

Having determined the nuclear structure of $Fe_2F_5(Htaz)$ in the non-centrosymmetric space group *Ima*2, we now turn to characterise the magnetic properties of this inorganic-organic hybrid coordination framework. Figure 3a shows the magnetic and inverse susceptibilities of $Fe_2F_5(Htaz)$ measured in an applied field of 0.1 T. Above 160 K, the inverse susceptibility follows a linear Curie-Weiss behaviour from which we extract a Curie constant, C = 8.91 emu K mol^{-1}, and a Weiss temperature, θ = –375(5) K. The effective paramagnetic moment extracted from the Curie constant, 8.44 μ_B per formula unit, compares well with that expected for a spin-only moment for Fe^{3+} but a significant orbital contribution to the Fe^{2+} moment. Crucially, the large and negative value of the Weiss temperature indicates that strong antiferromagnetic exchange interactions dominate. Upon cooling below 100 K, the magnetic susceptibility in Figure 3a exhibits a sharp increase, indicating the onset of long-range magnetic order at T_N = 93 K. The ratio between the energy scale for antiferromagnetic exchange, set by the Weiss temperature, and the Néel temperature gives a frustration index, $f = |\theta|/T_N \approx 4$, which reflects a modest frustration of the spin interactions within the triangular HTB layers. Below T_N, the ZFC and FC magnetic susceptibilities follow almost equal and opposite trends about either side of a compensation temperature, T^* = 34 K, at which point the susceptibilities pass through zero. Such behaviour is common in ferrimagnetic materials, arising from distinct temperature dependences of ordered moments on different magnetic sublattices.[29,30] The field dependence of the magnetisation, shown in Figure 3b, reveals that a ferromagnetic component exists in $Fe_2F_5(Htaz)$ above and below T^*, with a moment size of 0.07 μ_B mol^{-1} at both 4 K and 50 K. However, the coercive field increases from 0.22 T at 4 K to 0.41 T at 50 K.

Figures 3c and 3d show the temperature dependence of the magnetic susceptibility measured in an applied field of 1 T and 5 T, respectively. At 5 T, the negative magnetic susceptibility observed in weaker applied magnetic fields between T^* and T_N in the ZFC curve, and below T^* in the FC curve, has disappeared. Similar field variation of the magnetic response has been reported for other ferrimagnetic inorganic-organic hybrid coordination frameworks, including $AFe^{2+}Fe^{3+}(C_2O_4)_3$ (where A is an organic cation),[31] and the metal formate dihydrate, $M^{2+}(HCOO)_2.2H_2O$.[32,33] In the latter case, the observed behaviour was understood to arise from the antiferromagnetic coupling of two ferromagnetic M^{2+} sublattices. Here, we propose that in $Fe_2F_5(Htaz)$ the ferromagnetic Fe^{2+} and Fe^{3+} sublattices are antiferromagnetically coupled, which we confirm below through our analysis of low-temperature powder neutron diffraction data. The magnetisation of the ferromagnetic sublattices must evolve independently with temperature to allow for the compensation point, T^*, at which the ferromagnetic components on each of the sublattices exactly cancel.

Mössbauer Spectrometry

Figure 4 compares the ^{57}Fe Mössbauer spectra collected at 12 K in zero field and under an applied field of 8 T. As with previous measurements at 77 and 300 K on this and other related samples within the $M^{2+}M^{3+}F_5(Htaz)$ series, the hyperfine data characteristic of $Fe_2F_5(Htaz)$ at 12 K are consistent with a Fe^{2+}/Fe^{3+} ratio less than one.[13] This implies a small excess of Fe^{3+} ions within the structure, substituted on the Fe^{2+} 4*c* sites, which may be charge balanced by the deprotonation of the same fraction of H*taz* linker molecules. In the present case, the Mössbauer data indicate that the substitution of Fe^{3+} for Fe^{2+} is on the order of 4 %, such that the precise chemical composition is $(Fe^{2+}_{0.96}Fe^{3+}_{0.04})Fe^{3+}F_5(Htaz)_{0.96}(taz)_{0.04}$. However, as we concluded above, structural models of the idealised composition, $Fe_2F_5(Htaz)$, can be used to fit correctly the powder neutron diffraction data of our sample well.

In addition, the low-temperature Mössbauer spectrum of $Fe_2F_5(Htaz)$ measured in an 8 T field (Figure 4) is related to that of other fluoride weberites, such as $Fe_2F_5(H_2O)_2$.[34] In particular, the outer lines of the Fe^{3+} component are large and asymmetric. Such line shape broadening typically results from a distribution in the θ angle between the applied field and the hyperfine field, which is opposite to the magnetic moment. The asymmetry appears similar to that expected of a system with a sperimagnetic structure,[35] and in this case is consistent with a mean orientation of Fe^{3+} moments in $Fe_2F_5(Htaz)$ oriented in the opposite direction to the applied magnetic field. Such a structure differs from that observed in $Fe_2F_5(H_2O)_2$,[34] but, at this stage, one does consider how the application of an external magnetic field and the cooling conditions affect the hyperfine structure of $Fe_2F_5(Htaz)$. Indeed, the difference between zero field cooling and field cooling Mössbauer spectra result from the competition between the external magnetic field and the magnetic anisotropies, as it will be discussed in a forthcoming paper.

Magnetic Structure of $Fe_2F_5(Htaz)$

To rationalise the observed temperature and field dependent responses of $Fe_2F_5(Htaz)$ detailed above, and to correlate those behaviours with the underlying structure of the hybrid coordination framework, we finally outline our low-temperature powder neutron diffraction data and magnetic structure refinement. Figure 5 shows that upon cooling below T_N = 93 K, a significant increase in the intensities of several Bragg peaks at long *d*-spacing is observed in the powder neutron diffraction data of $Fe_2F_5(Htaz)$. This is consistent with the onset of long-range magnetic order. As the diffraction data measured below T_N can still be indexed by the nuclear *I*-centred cell, the propagation vector that describes the magnetic structure in $Fe_2F_5(Htaz)$ is $\boldsymbol{k}$ = (0, 0, 0). As has been previously reported for other fluoride weberites, $M^{2+}M^{3+}F_5(H_2O)_2$, the macroscopic theory of Bertaut can be employed to determine the possible magnetic modes for $Fe_2F_5(Htaz)$ that are compatible with the symmetry of its *Ima*2 nuclear structure and $\boldsymbol{k}$ = (0, 0, 0).[36] In this case, four possible linear combinations of the magnetic moments can be defined in each cation sublattice, shown in Table 4. However, the *C* and *A* configurations can be ruled out directly, since they are not compatible with the *I*-centred nuclear cell. Treating the symmetry elements of the *Ima*2 space group independently, and taking R_i and S_i (i = 1 – 4) as the magnetic moments M_i of the Fe^{3+} and Fe^{2+} ions, respectively, one can show that the basis vectors in the irreducible representation of the nuclear space group leads to four magnetic modes, Γ_i, that are compatible with a magnetisation on both sublattices. These are listed in Table 5. The existence of a ferromagnetic component in the magnetisation of $Fe_2F_5(Htaz)$ implies that the Γ_4 mode, which is purely antiferromagnetic, can be excluded as a possible description of the magnetic structure.

Rietveld refinement of the Γ_1, Γ_2 and Γ_3 modes against the powder neutron diffraction data collected at 2 K on GEM Bank 3 gave quality of fit parameters R_{wp} = 2.86 %, 3.57 % and 3.50 %, respectively. Figure 6 shows a plot of the best fit of the Γ_1 mode against the GEM Bank 3 data at 2 K, where the magnetic diffraction is most prominent. The quality of this fit indicates that Fe^{2+} sublattice is purely ferromagnetic, with a moment of 4.1(1) μ_B per Fe^{2+}. A small antiferromagnetic component, 0.6(3) μ_B, adds to the main ferromagnetic component of

Fe^{3+}, which aligns antiferromagnetically to the Fe^{2+} sublattice, as shown in Figure 7. The small size of the ferrimagnetic moment (0.07 μ_B mol^{-1} at 4 K from M vs H data) implies that the ferromagnetic F_z components of the Fe^{2+} and Fe^{3+} sublattices must be almost equal in magnitude and opposite in sign. In our initial treatment of the data, the ferromagnetic components of Fe^{3+} and Fe^{2+} were refined independently. However, the refinements were unstable and did not converge correctly, even when constrained to account for the observed compensation point at T^* = 34 K in the magnetic susceptibility data by fixing a difference of +0.07 μ_B and –0.07 μ_B between the magnitudes of the ferromagnetic F_z components of Fe^{3+} and Fe^{2+} sublattices at 2 K and 50 K, respectively. As a consequence, we have simply constrained the size of these components on each ion to be equal. This yields a magnetic moment of 4.3(1) μ_B for Fe^{3+} at 2 K, which is reduced from the full ordered moment of $\mu_{sat} = 2S = 5$ μ_B, but we note that such a moment reduction is observed in other frustrated spin systems. One pertinent example in the case is the Fe^{3+}-based fluoride FeF_3, which at 2 K has an ordered moment of 3.32 μ_B and 4.07 μ_B per Fe^{3+} in its pyrochlore and HTB phases, respectively.[37]

The successful refinement of the Γ_1 mode to the low temperature powder neutron diffraction data of $Fe_2F_5(Htaz)$ confirms that the Fe^{2+}–F–Fe^{3+} superexchange interactions are antiferromagnetic while the Fe^{3+}–F–Fe^{3+} interactions must be predominantly ferromagnetic. It is interesting, therefore, to compare this configuration with those found in the inorganic fluoride weberite Na_2NiFeF_7 below T_N = 88 K,[23] and in the magnetic structures of $Fe_2F_5(H_2O)_2$.[21] In the case of Na_2NiFeF_7, there is no antiferromagnetic component in the ordered ground state, but the system adopts a similar collinear ferrimagnetic model. In $Fe_2F_5(H_2O)_2$, on the other hand, a relatively larger antiferromagnetic component of 1.6 μ_B exists on the Fe^{2+} sublattice, with ferromagnetic components aligned perpendicular to the Fe^{3+} chains below T_N = 46 K. However, $Fe_2F_5(H_2O)_2$ displays a more complex temperature evolution than is the case for $Fe_2F_5(Htaz)$, as it undergoes a second magnetic phase transition below 26 K in which the Fe^{3+}–F–Fe^{3+} coupling induces a pronounced canting of the Fe^{3+} moments. In the case $Fe_2F_5(Htaz)$, it is likely too that the interactions between the Fe^{3+} cations in the $_\infty[Fe^{3+}F_5]$ chains become increasingly antiferromagnetic as the system is cooled, causing the Fe^{3+} moments to be canted in a similar mechanism to that observed in $Fe_2F_5(H_2O)_2$.[20]

Conclusions

In summary, we have shown that the inorganic-organic hybrid fluoride $Fe_2F_5(Htaz)$ adopts a weberite-type structure with HTB layers of six-fold coordinate Fe^{2+} and Fe^{3+} cations. Contrary to our previous understanding from X-ray diffraction data, our powder neutron diffraction study reveals that the structure of $Fe_2F_5(Htaz)$ is best described in the non-centrosymmetric orthorhombic space group *Ima*2 at room temperature, rather than in the centrosymmetric *Imma* space group that represents the structure of related $Fe_2F_5(H_2O)_2$. ^{57}Fe Mössbauer spectrometry shows that the Fe^{2+}/Fe^{3+} ratio is ~ 0.92, which is likely charge balanced by the deprotonation of the H*taz* linker molecules within the hybrid framework, and as such, $Fe_2F_5(Htaz)$ represents the idealised formula of the title compound. Our magnetic susceptibility measurements reveal that strong antiferromagnetic interactions dominate in $Fe_2F_5(Htaz)$, with a Weiss temperature θ = –375(5) K, leading to a magnetic ordering transition at T_N = 93 K. Magnetisation data indicate that a small ferrimagnetic component exists below T_N which results from the vector sum of the antiparallel ferromagnetic components oriented along the *c*-axis of the Fe^{2+} and Fe^{3+} sublattices, as our low-temperature powder neutron diffraction data suggest. Under an applied field of 0.1 T, the orientation of the ferrimagnetic component inverts at T^* ~ 34 K, giving rise to a negative magnetic susceptibility. Increasing the applied magnetic field strength suppresses this negative susceptibility, such that it is almost completely removed under a field of 1 T. The existence of the compensation point in the magnetic susceptibility of $Fe_2F_5(Htaz)$ is a common feature of ferrimagnetic solids, which in this case arises due to the different temperature evolution of Fe^{2+} and Fe^{3+} sublattice magnetisations and the anisotropy of the Fe^{2+} ions that restricts the orientation of its magnetic moment. The successful

refinement of the Γ_1 magnetic mode to describe the magnetic ordering on both magnetic sublattices in $Fe_2F_5(Htaz)$ implies that the 180°-type antiferromagnetic superexchange interactions between Fe^{2+} and Fe^{3+} are satisfied but that the 180°-type Fe^{3+}–F–Fe^{3+} interactions are predominantly ferromagnetic. Only a small antiferromagnetic component appears for Fe^{3+} along the *b*-axis, and we suggest these unusual features are a key manifestation of the frustrated nature of the magnetic interactions in the HTB layers of $Fe_2F_5(Htaz)$. In addition, one can imagine that the cationic disorder in the system – as revealed by ^{57}Fe Mössbauer spectrometry – combined with the inherent frustration of the HTB-type lattice of the weberite structure may lead to spin-glass like behaviour in $Fe_2F_5(Htaz)$. While this is not immediately apparent in our current investigation, future AC susceptibility measurements, or local magnetic structure probes such as muon spectroscopy and magnetic diffuse neutron scattering could perhaps reveal glassy dynamics around the magnetic ordering transition in $Fe_2F_5(Htaz)$.

Finally, it is important to consider the extent to which the structure-function analogies one can draw between this strongly interacting hybrid framework material and purely inorganic solids have helped us in understanding the properties of this new material. Certainly, $Fe_2F_5(Htaz)$ stands out as a novel hybrid system that acts to dispel the notion that magnetic interactions in framework materials are necessarily weak, as it mimics the cooperative magnetic phenomena typical of inorganic solids on a comparable energy scale. And indeed, prior knowledge of the magnetic ordering in the related inorganic compounds has aided our ability to rationalise the observed behaviour in $Fe_2F_5(Htaz)$ as they are similar, but crucially, they are not the same. As such, $Fe_2F_5(Htaz)$ also serves as a useful illustration of the additional flexibility that can be bestowed upon a hybrid framework, in comparison to its inorganic counterparts, through its organic linker molecules that can give rise to new structural features or functionality. In the case of $Fe_2F_5(Htaz)$, the arrangement of the H*taz* linkers gives rise to a previously unreported non-centrosymmetric structure. This furthermore highlights the unique insight afforded by neutron diffraction for the study of hybrid materials, which in the case of the structure solution of $Fe_2F_5(Htaz)$, was critical. As hybrid materials continue to be at the fore of materials research for their remarkable photovoltaic, catalytic and magnetic properties, it perhaps noteworthy to the wider community that such valuable information can still be extracted from powder neutron diffraction data of inorganic-organic frameworks without the need for costly deuteration when the relative number of hydrogen atoms is small.

Additional Information

Funding Statement and Acknowledgements
LC acknowledges the University of Liverpool for start-up funding and support. Work at the University of St Andrews was supported by a Leverhulme Research Project Grant. Access to beam time at the ISIS Neutron and Muon Facility was supported by the Science and Technology Facilities Council. The authors also gratefully acknowledge Delphine Toulemon, ITODYS, UMR7086 CNRS, Université Paris VII, for assistance with magnetisation measurements.

Data Accessibility
All requests for data should be made to the corresponding author, with the exception of the GEM powder neutron diffraction data, which can be found at DOI: 10.5286/ISIS.E.60997113.

Competing Interests
The authors have no competing interests.

Authors' Contributions

LC, MA and IdS and collected the neutron diffraction data, which were analysed by LC, MA and ML. LC and CP collected the magnetometry data and analysed them with MA, PL and ML. MA, VP prepared the sample under the guidance of JL, VM and ML, who conceived our wider investigation of the inorganic-organic hybrid weberite fluorides. J-MG collected and analysed Mössbauer spectroscopy data. LC and ML wrote the manuscript, which all authors have read and approved.

References

1. Leblanc M, Maisonneuve V, Tressaud A. 2015. Crystal Chemistry and Selected Physical Properties of Inorganic Fluorides and Oxide-Fluorides. *Chem. Rev.* **115**, 1191-1254. (doi: 10.1021/cr500173c)
2. Lake B, Tennant DA, Frost CD, Nagler SE. 2005. Quantum criticality and universal scaling of a quantum antiferromagnet. *Nature Mater.* **4**, 329-334. (doi: 10.1327/nmat1327)
3. Ederer C, Spaldin NA. 2006. Origin of ferroelectricity in the multiferroic barium fluorides BaMF$_4$: A first principles study. *Phys. Rev. B* **74**, 024102. (doi: 10.1103/PhysRevB.74.024102)
4. Düvel A, Bednarcik J, Sepelák V, Heitjans P. 2014. Mechanosynthesis of the Fast Fluoride Ion Conductor Ba$_{1-x}$La$_x$F$_{2+x}$: From the Fluorite to the Tysonite Structure. *J. Phys. Chem. C* **118**, 7117-7129. (doi: 10.1021/jp410018t)
5. Pedersen KS, Sørensen MA, Bendix J. 2015. Fluoride-coordination chemistry in molecular and low-dimensional magnetism. *Coord. Chem. Rev.* **299**, 1- 21. (doi: 10.1016/j.ccr.2015.03.024)
6. Huang Y-B, Liang J, Wang X-S, Cao R. 2017. Multifunctional metal-organic framework catalysts: synergistic catalysis and tandem reactions. *Chem. Rev. Soc.* **46**, 126-157. (doi: 10.1039/c6cs00250a)
7. Li H, Wang K, Sun Y, Lollar CT, Li J, Zhou H-C. 2018. Recent advances in gas storage and separation using metal-organic frameworks. *Materials Today* **21**, 108-121. (doi: 10.1016/j.mattod.2017.07.006)
8. McKinlay AC, Morris RE, Horcajada P, Férey G, Gref R, Couvreur P, Serre C. 2010. BioMOFs: Metal-Organic Frameworks for Biological and Medical Applications. *Angew. Chem. Int. Ed.* **49**, 6260-6266. (doi: 10.1002/anie.201000048)
9. Cliffe MJ, Lee J, Paddison JAM, Schott S, Mukherjee P, Gaultois MW, Manuel P, Sirringhaus H, Dutton SE, Grey CP. 2018. Low-dimensional quantum magnetism in Cu(NCS)$_2$: A molecular framework material. *Phys. Rev. B* **97**, 144421. (doi: 10.1103/PhysRevB.97.144421)
10. Walker HC, Duncan HD, Le MD, Keen DA, Voneshen DJ, Phillips AE. 2017. Magnetic structure and spin-wave excitations in the multiferroic magnetic metal-organic framework (CD$_3$)$_2$ND$_2$[Mn(DCO$_2$)$_3$]. *Phys. Rev. B* **96**, 094423. (doi: 10.1103/PhysRevB.96.094423)
11. Yamada MG, Fujita H, Oshikawa M. 2017. Designing Kitaev Spin Liquids in Metal-Organic Frameworks. *Phys. Rev. Lett.* **119**, 057202. (doi: 10.1103/PhysRevLett.119.057202)
12. Clark L, Aidoudi FH, Black C, Arachchige KSA, Slawin AMZ, Morris RE, Lightfoot P. 2015. Extending the Family of V^{4+} S = 1/2 Kagome Antiferromagnets. *Angew. Chem. Int. Ed.* **127**, 15677-15681. (doi: 10.1002/ange.201506869)
13. Albino M, Clark L, Lhoste J, Payen C, Grenèche JM, Lightfoot P, Maisonneuve V, Leblanc M. 2017 A magnetisation and Mössbauer study of triazole (M$_{1-x}^{2+}$M$_x^{3+}$)M^{3+}F$_5$(H*taz*)$_{1-x}$(*taz*)$_x$ weberites (M = Fe, Co, Mn, Zn, Ga, V). *Dalton Trans.* **46**, 5352-5362. (doi:10.1039/c7dt00587c)
14. Smida M, Lhoste J, Pimenta V, Hémon-Ribaud A, Jouffret L, Leblanc M, Dammak M, Grenèche JM, Maisonneuve V. 2013 New series of hybrid fluoroferrates synthesized with triazoles: various dimensionalities and Mössbauer studies. *Dalton Trans.* **42**, 15748-15755. (doi:10.1039/c3dt51812d)
15. Cadiau A, Martineau C, Leblanc M, Maisonneuve V, Hémon-Ribaud A, Taulelle F, Adil K. 2011 ZnAlF$_5$·[*taz*]: an Al fluorinated MOF of MIL-53(Al) topology with cationic {Zn(1,2,4 triazole)}$^{2+}$ linkers. *J. Mater. Chem.* **21**, 3949-3951. (doi: 10.1039/c0jm03559a)

16. Yakubovich O, Urusov V, Massa W, Frenzen G, Babel D. 1993 Structure of $Na_2Fe_2F_7$ and structural relations in the family of weberites $Na_2M^{II}M^{III}F_7$. *Z. Anorg. Allg. Chem.* **619**, 1909-1919. (doi: 10.1002/zaac.19936191115)
17. Babel D, Tressaud A. 1985. Crystal chemistry of fluorides. In *Inorganic Solid Fluorides* (ed. P Hagenmuller), pp. 77-203. Academic Press. (doi : 10.1016/B978-0-12-313370-0.50008-6)
18. Tressaud A, Dance JM, Portier J, Hagenmuller P. 1974 Interactions magnétiques dans les fluorures de type weberite. *Mater. Res. Bull.* **9**, 1219-1226. (doi: 10.1016/0025-5408(74)90040-3)
19. Laligant Y, Pannetier J, Labbe P, Férey G. 1986 A new refinement of the crystal structure of the inverse weberite $Fe_2F_5(H_2O)_2$. *J. Solid State Chem.* **62**, 274-277. (doi: 10.1016/0022-4596(86)90240-9)
20. Laligant Y, Leblanc M, Pannetier J, Férey G. 1986 Ordered magnetic frustration: IV. The two magnetic structures of the inverse weberite $Fe_2F_5(H_2O)_2$: an example of the thermal evolution of the frustration character. *J. Phys. C Solid State* **19**, 1081-1095. (doi: 10.1088/0022-3719/19/8/007)
21. Férey G, Leblanc M, De Pape R, Pannetier J. 1985 Competing spin interactions and frustration effects in fluorides. In *Inorganic Solid Fluorides* (ed. P Hagenmuller), pp. 395-414. London: Academic Press. (doi: 10.1016/B978-0-12-313370-0.50015-3)
22. Dance JM, Tressaud A. Ferro- and ferrimagnetism in fluorides. In *Inorganic Solid Fluorides* (ed. P Hagenmuller), pp. 371-394. London: Academic Press. (doi:10.1016/B978-0-12-313370-0.50014-1)
23. Laligant Y, Calage Y, Heger G, Pannetier J, Ferey G. 1989 Ordered Magnetic Frustration. VII. Na_2NiFeF_7: Reexamination of its crystal structure in the true space group after corrections from Renninger effect and refinement of its frustrated magnetic structure at 4.2 and 55 K. *J. Solid State Chem.* **78**, 66-75. (doi: 10.1016/0022-4596(89)90128-X)
24. Schmidt R.E, Massa W, Babel D. 1992 Die kristallstruktur von Na_2NiAlF_7 - ein beitrag zum problem der wahren raumgruppe orthorhombischer weberite. *Z. Anorg. Allg. Chem.* **615**, 11-15. (doi: 10.1002/zaac.19926150903)
25. Laligant Y, Pannetier J, Leblanc M, Labbé P, Hegger G, Férey G. 1987 Crystal structure refinement of the inverse weberite $MnFeF_5(H_2O)_2$ *Z. Kristallogr.* **181**, 1-10. (doi: 10.1524/zkri.1987.181.14.1.)
26. Laligant Y, Calage Y, Torres-Tapia E, Grenèche JM, Varret F, Férey G. 1986 Crystal structure of the inverse weberite $ZnFeF_5(H_2O)_2$, magnetic and Mössbauer study of the antiferromagnet $ZnFeF_5(H_2O)_2$ and ferrimagnet $MnFeF_5(H_2O)_2$. *J. Magn. Magn. Mater.* **61**, 283-290. (doi: 10.1016/0304-8853(86)90040-5)
27. Leblanc M, Pannetier J, Férey G, De Pape R. 1985 Single crystal refinement of the structure of rhombohedral iron trifluoride. *Rev. Chim. Miner.* **22**, 107-114.
28. Stout JW, Reed SA. 1954 The crystal structure of MnF_2, FeF_2, CoF_2, NiF_2 and ZnF_2. *J. Am. Chem. Soc.* **76**, 5279-5281. (doi:10.1021/ja01650a005)
29. Spaldin NA. 2011 In Magnetic materials fundamentals and applications, pp. 112 – 127. Cambridge University Press.
30. Kumar A, Yusuf SM. 2015 The phenomenon of negative magnetization and its implications. *Phys. Rep.* **556**, 1-34. (https://doi.org/10.1016/j.physrep.2014.10.003)
31. Nuttall CJ, Day P. 1998 Magnetization of the layer compounds $A Fe^{II}Fe^{III}(C_2O_4)_3$ (A = Organic cation), in low and high magnetic fields: manifestation of Néel N and Q type ferrimagnetism in a molecular lattice. *Chem. Mater.* **10**, 3050-3057. (doi: 10.1021/cm980177g)
32. Kageyama H, Khomskii DI, Levitin RZ, Vasilev AN. 2003 Weak ferrimagnetism, compensation point, and magnetization reversal in $Ni(HCOO)_2{\cdot}2H_2O$. *Phys. Rev. B* **67**, 224422. (doi: 10.1103/PhysRevB.67.224422)

33. Kellerman DG, Barykina YA, Zheleznikov KA, Tyutyunnik AP, Krasilnikov VN. 2016 Magnetic ordering in dihydrated formates $M(HCOO)_2 \cdot 2H_2O$, M = Mn, Fe, Co, Ni: DC magnetization study. *Phys. Status Solidi B* 1-8. (doi: 10.1002/pssb.201600107)
34. Grenèche JM, Linares, Varret F, Laligant Y, Férey G. 1988 Mössbauer spectroscopy of the magnetic behaviour of the frustrated series $AFeF_5(H_2O)_2$: A= Mn, Fe, Co, Ni. *J. Magn. Magn. Mater.* **73**, 115-122. (doi.org/10.1016/0304-8853(88)90177-1)
35. Grenèche JM. (2013) The contribution of ^{57}Fe Mössbauer spectrometry to investigate magnetic nanomaterials, *in Mössbauer Spectroscopy* (ed. Y Yoshida and G Langouche), pp. 187-241. Springer Berlin Heidelberg and references therein. (doi: 10.1007/978-3-642-32220-4_4)
36. Bertaut EF. 1963 In Magnetism III (ed. GT Rado, H Suhl), pp. 147. New York: Academic Press.
37. Férey G, De Pape R, Leblanc M, Pannetier J. 1986 Ordered magnetic frustration: VIII. Crystal and magnetic structures of the pyrochlore form of FeF_3 between 2.5 and 25K from powder neutron diffraction. Comparison with the other varieties of FeF_3. *Rev. Chim. Miner.* **23**, 474-484.

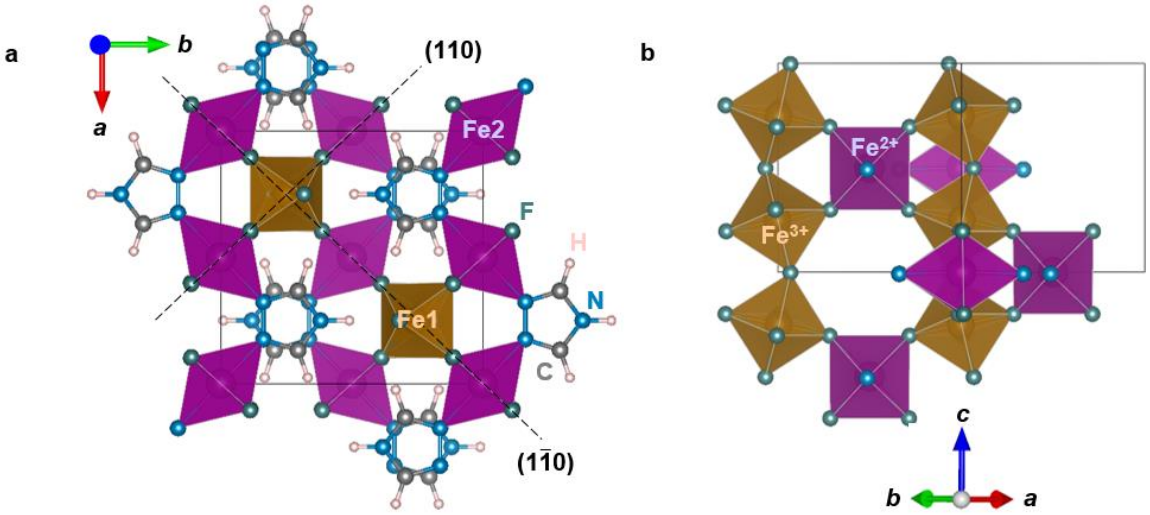

Figure 1. (a) A projection of the refined *Ima*2 structure of $Fe_2F_5(Htaz)$ showing the nearly orthogonal HTB layers in the (110) and (1$\bar{1}$0) type planes **(b)** that contain a triangular network of Fe^{3+} (site 4*b*) and Fe^{2+} (site 4*a*) cations connected via fluoride anions.

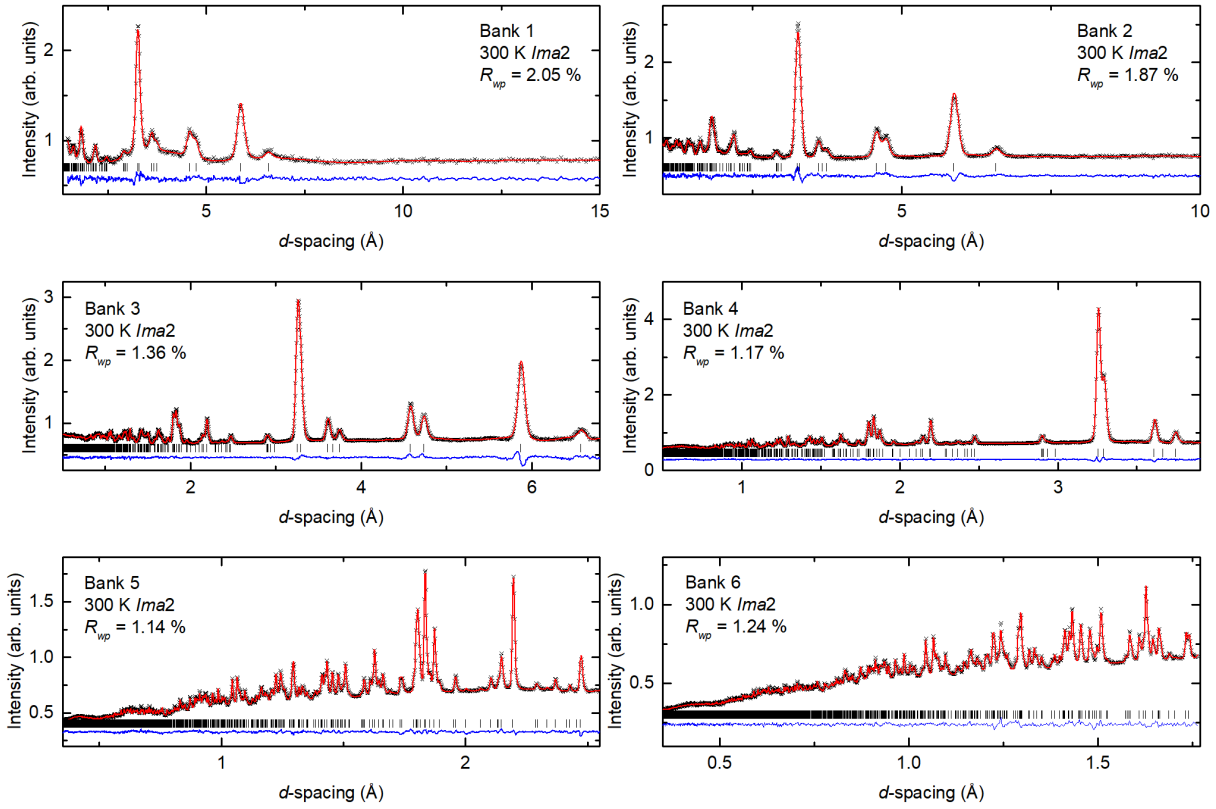

Figure 2. Rietveld refinement of the isotropic *Ima*2 structural model of $Fe_2F_5(Htaz)$ to powder neutron diffraction data collected on each of the six detector banks on the GEM diffractometer at 300 K with a total R_{wp} = 1.26 %.

Table 1. Isotropic (R_{wp} = 1.37 %) and anisotropic (R_{wp} = 1.11 %) *Imma* structural models refined to the powder neutron diffraction data collected at 300 K for $Fe_2F_5(Htaz)$. Refined lattice parameters for the centrosymmetric orthorhombic unit cell are a = 9.1469(2) Å, b = 7.4828(1) Å and c = 9.4640(2) Å.

Atom	Position	x	y	z	U_{iso} / Å²	U_{11} / Å²	U_{22} / Å²	U_{33} / Å²	U_{12} / Å²	U_{13} / Å²	U_{33} / Å²
Fe1	4*a*	½	½	½	0.0040(3)	–	–	–	–	–	–
Fe2	4*c*	¾	¾	¾	0.0088(4)	–	–	–	–	–	–
F2	4*e*	½	¾	0.4328(2)	0.0117(6)	–	–	–	–	–	–
F2	16*j*	0.6467(1)	0.5514(2)	0.6367(1)	0.0138(3)	–	–	–	–	–	–
N1	8*i*	0.9255(1)	¾	0.5869(1)	0.0155(4)	0.0111(5)	0.0262(8)	0.0095(6)	0.00	0.0034(4)	0.00
N2	4*e*	0	¾	0.3706(1)	0.0222(6)	0.021(1)	0.048(8)	0.0045(8)	0.00	0.00	0.00
C1	8*i*	0.8853(2)	¾	0.4550(1)	0.0191(6)	0.0065(9)	0.071(2)	0.0069(9)	0.00	–0.0057(6)	0.00
H1	8*i*	0.7706(4)	¾	0.4184(4)	0.066(2)	0.0030(2)	0.227(6)	0.031(3)	0.00	–0.007(2)	0.00
H2	4*e*	0	¾	0.2597(5)	0.048(2)	0.038(4)	0.168(2)	0.015(3)	0.00	0.00	0.00

Table 2. Isotropic (R_{wp} = 1.26 %) *Ima*2 structural model refined to the powder neutron diffraction data collected at 300 K for $Fe_2F_5(Htaz)$. Refined lattice parameters for the non-centrosymmetric orthorhombic unit cell are a = 9.1467(2) Å, b = 9.4641(2) Å and c = 7.4829(2) Å. The z-coordinate of the Fe2 site has been fixed to define the unit cell origin.

Atom	Position	x	y	z	U_{iso} / Å^2
Fe1	4*b*	¼	0.2525 (6)	0.2529(9)	0.0037(4)
Fe2	4*a*	0	0	0	0.0088(4)
F1	4*b*	¼	0.3191(3)	0.0036(13)	0.0138(7)
F2	8*c*	0.1013(7)	0.1128(6)	0.2024(9)	0.0076(9)
F3	8*c*	0.1045(7)	0.3863(8)	0.3049(9)	0.0240(13)
N1	8*c*	0.1757(1)	-0.1625(1)	0.0120(8)	0.0145(4)
N2	4*b*	¼	0.6194(2)	0.0175(9)	0.0180(6)
C1	8*c*	0.1329(2)	0.7058(2)	–0.0184(9)	0.0120(6)
H1	8*c*	0.0224(5)	0.6679(4)	–0.0351(9)	0.0377(17)
H2	4*b*	¼	0.5103(6)	–0.0254(15)	0.0372(20)

Table 3. Selected bond distances and angles taken from the refinement of the *Ima*2 structural model to powder neutron diffraction data collected for $Fe_2F_5(H$*taz*) at 300 K.

Bond	**Bond length / Å**	**Bond**	**Bond length / Å**
Fe1-F2 × 2	1.934(9)	Fe2-F2 × 2	2.072(6)
Fe1-F3 × 2	1.877(9)	Fe2-F3 × 2	2.050(7)
Fe1-F1 × 1	1.969(10)	Fe2-N1 × 2	2.226(1)
Fe1-F1 × 1	1.995(10)	<Fe2-F>	2.116
<Fe1-F>	1.931		
X-H···F (X = N, C)	**X-H / Å**	**H···F / Å**	**X···F / Å**
N2-H2···F1	1.081(8)	1.822(7)	2.843(3)
C1-H1···F3	1.080(6)	2.326(7)	3.204(7)
Bond		**Angle / °**	
Fe1-F1-Fe1		141.4(1)	
Fe1-F2-Fe2		144.0(3)	
Fe1-F3-Fe2		146.3(3)	
N2-H2···F1		155.8(9)	
C1-H1···F3		168.7(2)	

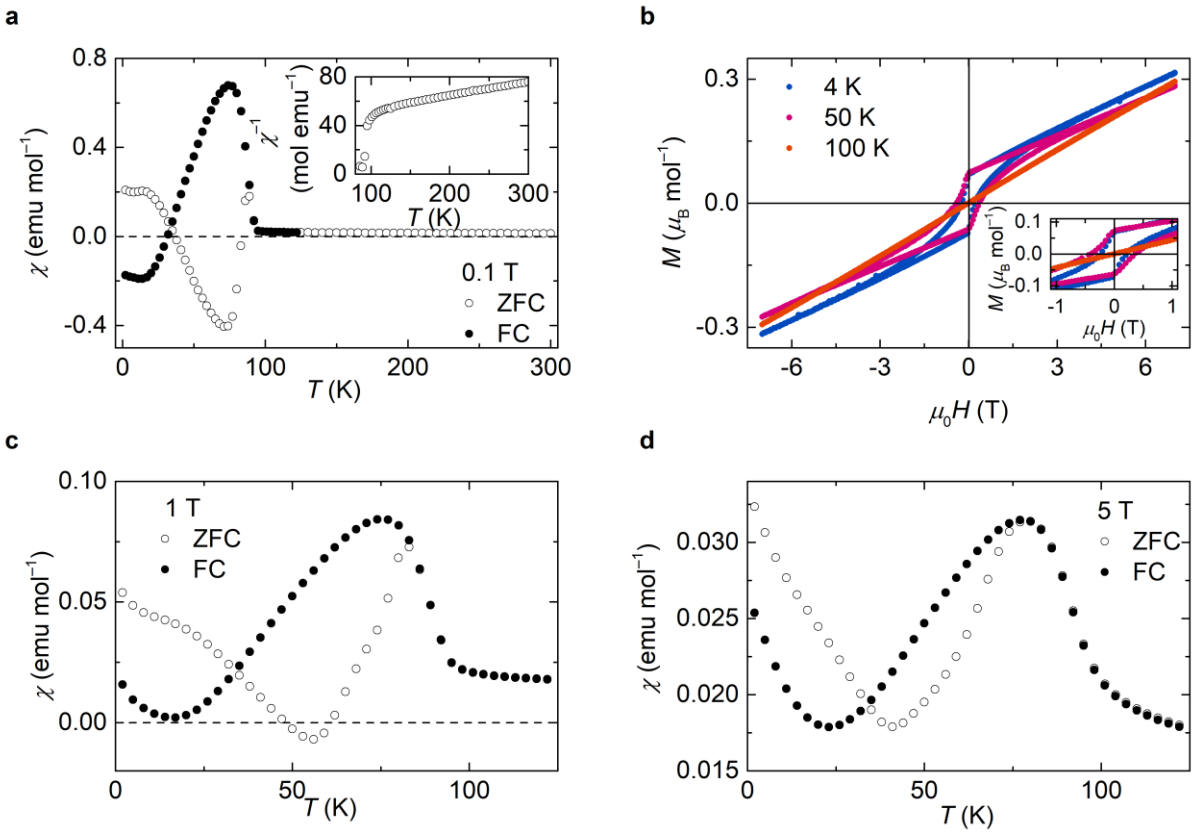

Figure 3. (a) Temperature dependence of the zero-field cooled (ZFC) and field cooled (FC) susceptibilities of $Fe_2F_5(Htaz)$ at 0.1 T, the inset shows Curie-Weiss behaviour in the high-temperature inverse susceptibility. **(b)** Magnetisation *vs.* field loops measured at 4 K, 50 K and 100 K, the inset shows an enlargement of the data at low fields. Temperature dependence of the ZFC and FC susceptibilities measured in fields of **(c)** 1 T and **(d)** 5 T.

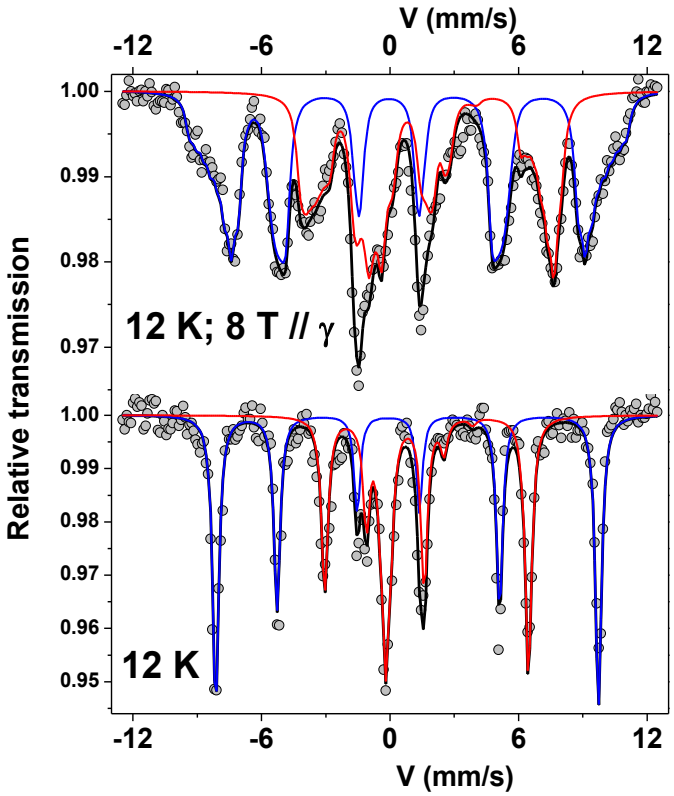

Figure 4. ^{57}Fe Mössbauer spectra of $Fe_2F_5(Htaz)$ at 12 K in **(bottom)** zero field and **(top)** an applied field of 8 T. The blue and red lines correspond to Fe^{3+} and Fe^{2+} magnetic components, respectively.

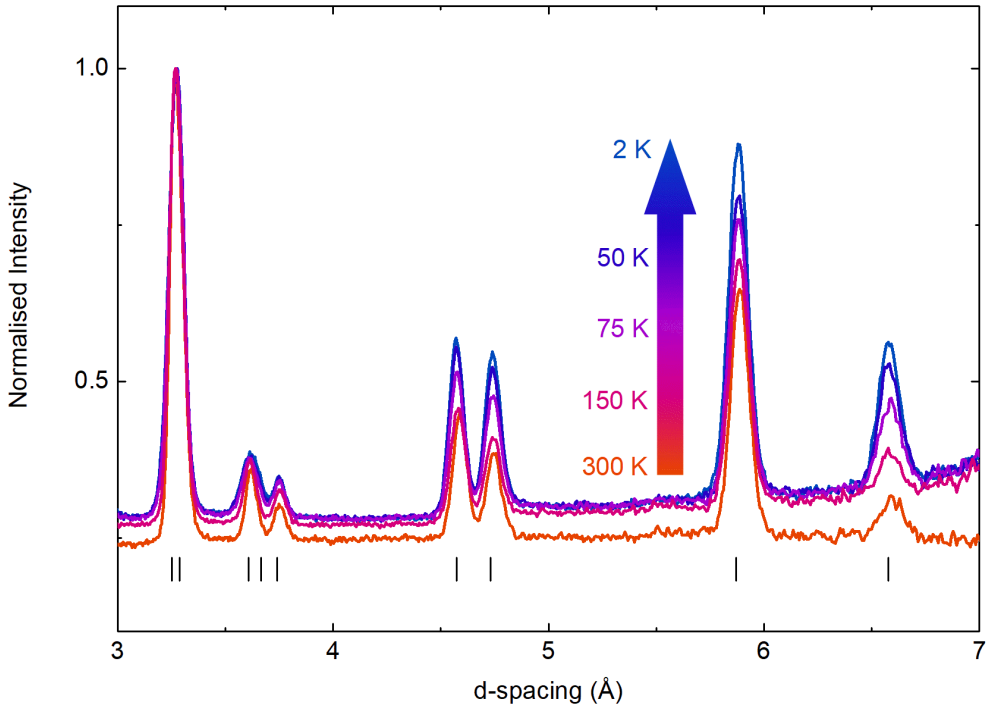

Figure 5. Variation in the normalised Bragg peak intensity measured in GEM Bank 3 upon cooling through T_N = 93 K. Tick marks show the nuclear allowed reflection positions for the *Ima*2 cell.

Table 4. Ferromagnetic and antiferromagnetic configurations of the magnetic moments.

F	=	M_1	+	M_2	+	M_3	+	M_4
G	=	M_1	−	M_2	+	M_3	−	M_4
C	=	M_1	+	M_2	−	M_3	−	M_4
A	=	M_1	−	M_2	−	M_3	+	M_4

Table 5. Coordinates of the magnetic ions S_i (Fe^{2+}) and R_i (Fe^{3+}) in $Fe_2F_5(Htaz)$ and their irreducible representations in the nuclear space group *Ima*2.

	Fe^{3+}				Fe^{2+}		
$\boldsymbol{R_1}$	¼	¼	¼	$\boldsymbol{S_1}$	0	0	0
$\boldsymbol{R_2}$	¾	¾	¼	$\boldsymbol{S_2}$	½	0	0
$\boldsymbol{R_3}$	¾	¾	¾	$\boldsymbol{S_3}$	½	½	½
$\boldsymbol{R_4}$	¼	¼	¾	$\boldsymbol{S_4}$	0	½	½
Mode	$\boldsymbol{x}$	$\boldsymbol{y}$	$\boldsymbol{z}$		$\boldsymbol{x}$	$\boldsymbol{y}$	$\boldsymbol{z}$
$\boldsymbol{\Gamma_1}$		G_y	F_z				F_z
$\boldsymbol{\Gamma_2}$		F_y	G_z		G_x	F_y	
$\boldsymbol{\Gamma_3}$	F_x				F_x	G_y	
$\boldsymbol{\Gamma_4}$	G_x						G_z

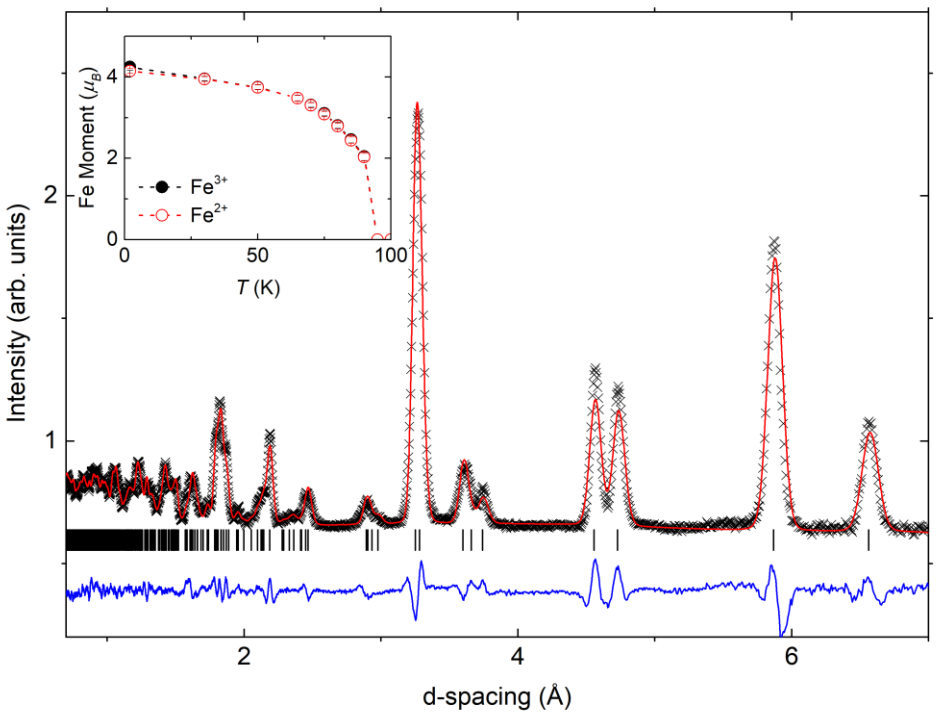

Figure 6. Rietveld refinement of the Γ_1 magnetic mode to powder neutron diffraction data collected on Bank 3 of the GEM diffractometer at 2 K to describe the magnetic ordering of the Fe^{2+} and Fe^{3+} sublattices in the *Ima*2 nuclear space group. R_{wp} = 2.86 %, a = 9.1199(9) Å, b = 9.4499(9) Å, c = 7.4775(5) Å. The inset shows the temperature evolution of the magnitude of the refined total magnetic moments on the Fe^{3+} and Fe^{2+} sublattices below T_N = 93 K, from the model in which their ferromagnetic components are constrained to be equal.

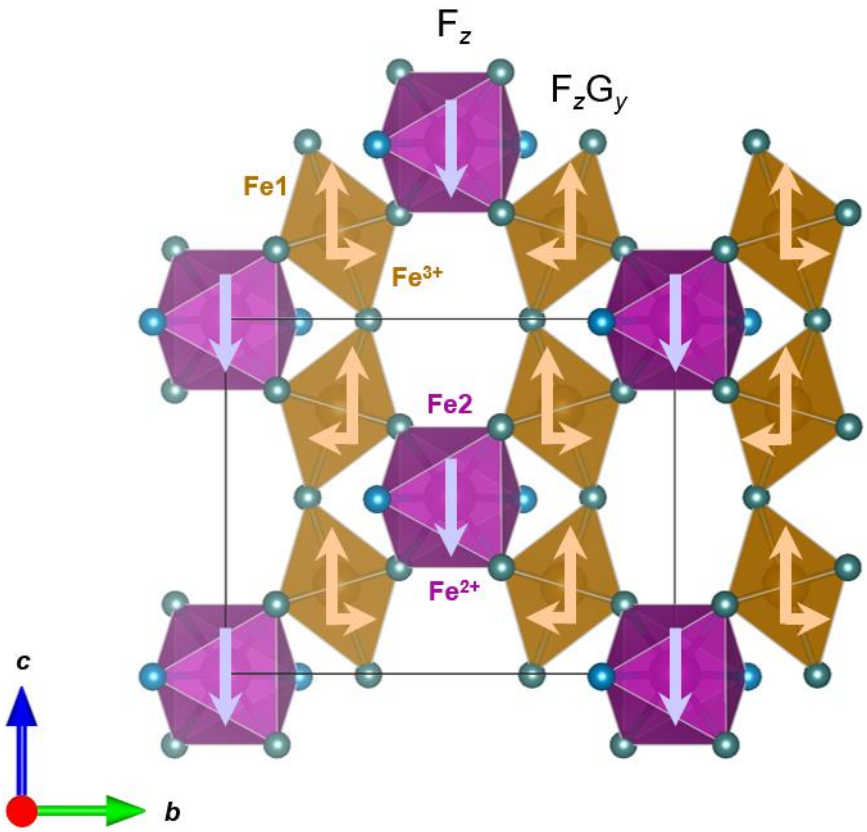

Figure 7. Magnetic modes of $Fe_2F_5(Htaz)$ represented on the HTB layer in the $(1\bar{1}0)$ plane and projected along the [100] direction.